Jurnal Dinamis (*Scientific Journal of Mechanical Engineering*)
Journal homepage: https://talenta.usu.ac.id/dinamis/

Erosion Behavior of SKD11 Tool Steel Under Different Impact Angles and Particle Velocities: A Finite Element Analysis Study

Deva Ihsan Khoirunas[1], Riki Hendra Purba[*1], Riky Stepanus Situmorang[2], James Julian[1], Fitri Wahyuni[1], Elvi Armadani[1], Fathin Muhammad Mardhudhu[1]
[1]*Mechanical Engineering Department, Universitas Pembangunan Nasional Veteran Jakarta, 12450, Indonesia;*
[2]*Mechanical Engineering Department, Universitas Sumatera Utara, Indonesia;*

[*]Corresponding Author: rikihendrapurba@upnvj.ac.id

ARTICLE INFO

Article history:
Received November 4th 2025
Revised December 27th 2025
Accepted December 29th 2025
Available online December 31th 2025

E-ISSN: 2809-3410

How to cite:
Deva Ihsan Khoirunas, Riki Hendra Purba, Riky Stepanus Situmorang, James Julian, Fitri Wahyuni, Elvi Armadani, Fathin Muhammad Mardhudhu, "Erosion Behavior of SKD11 Tool Steel Under Different Impact Angles and Particle Velocities: A Finite Element Analysis Study," *Junal Dinamis (Scientific Journal of Mechanical Engineering)*, Vol. 13, No. 2, pp. 99-106, December 2025.

ABSTRACT

This study aims to numerically investigate the erosion response and underlying damage mechanisms of SKD11 tool steel under varying particle impact angles and velocities. The study utilizes the Single Particle Finite Element Analysis (FEA) method with a Cowper-Symonds Strain Rate Material Model. In this study, SiO_2 particles measuring 0.7 mm in diameter were selected as the erodent, while the target material, SKD11, was sized at 1x1x0,5 mm. The impact angle was varied at 30, 60, and 90 degrees, and the impact velocity was set at 25 and 50 m/s. The simulation results indicate that SKD11 exhibits the highest resistance to erosion at lower impact angles. Erosion severity increases markedly as the impact angle rises, reaching a maximum at 60°. Moreover, different impact angles lead to distinct erosion mechanisms on the material surface. Increasing the particle velocity further intensifies erosion, with material failure and removal observed at 50 m/s. These findings provide insight into the combined effects of impact angle and velocity on erosion behavior and contribute to improved prediction and design of erosion-resistant SKD11 components.

Keyword: *Erosion model, Finite Element Analysis, SKD11, Tool* steel

ABSTRAK

Penelitian ini bertujuan untuk mengkaji secara numerik respons serta mekanisme erosi pada baja perkakas SKD11 dengan beberapa variasi sudut dan kecepatan tumbukan partikel. Metode Single Particle Finite Element Analysis (FEA) dengan model material Cowper–Symonds strain rate dependent digunakan dalam penelitian ini. Pada studi ini partikel SiO_2 berdiameter 0,7 mm dipilih sebagai eroden dengan target material SKD11 berukuran 1x1x0,5 mm. Sudut serang divariasikan sebesar 30, 60, dan 90 derajat dengan kecepatan tumbukan divariasikan sebesar 25 dan 50 m/s. Hasil simulasi menunjukkan bahwa SKD11 memiliki ketahanan erosi tertinggi pada sudut tumbukan yang rendah. Laju erosi meningkat secara signifikan seiring dengan meningkatnya sudut tumbukan dan mencapai nilai maksimum pada sudut 60°. Selain itu, perbedaan sudut tumbukan menghasilkan mekanisme erosi yang berbeda pada permukaan material. Peningkatan kecepatan partikel juga memengaruhi erosi yang terjadi, yang ditandai dengan terjadinya kegagalan dan pelepasan material ketika kecepatan ditingkatkan ke 50 m/s. Temuan ini memberikan pemahaman mengenai pengaruh gabungan sudut dan kecepatan tumbukan terhadap perilaku erosi, serta berkontribusi pada peningkatan prediksi dan perancangan komponen SKD11 yang lebih tahan terhadap erosi.

Keyword: Baja perkakas, Metode elemen hingga, Model erosi, SKD11

http://doi.org/10.32734/dinamis.v13i2.23396

1. Introduction

Erosion is a phenomenon that occurs when a material undergoes repeated impacts from high-velocity particles. Over time, these impacts lead to surface degradation and material loss. This process is a significant challenge in the heavy equipment industry, particularly in operations under extreme conditions [1], [2], [3].

Tool steel is a fundamental material in the metal forming industry, die manufacturing, and cutting tool production due to its superior mechanical properties. The efficiency and effectiveness of metal forming processes can be significantly enhanced by selecting materials with optimal mechanical characteristics. Among the widely utilized tool steels, JIS SKD11, also known as AISI D2 stands out as a preferred choice. Its exceptional hardness and high wear resistance make it particularly well-suited for demanding industrial applications, ensuring durability and prolonged service life in extreme operating conditions [4], [5], [6], [7], [8], [9], [10].

Erosion in SKD11 steel can be attributed to various factors, including friction with other materials, exposure to corrosive environments, and abrasive forces during operation. Developing wear-resistant materials is crucial for enhancing tool longevity and improving production efficiency, ultimately reducing operational costs [11]. Numerical analysis using the Finite Element Method (FEA) has become increasingly prevalent in research and development due to its several advantages over experimental approaches, such as lower costs and faster processing times [12].

Yaer et al. (2019) conducted a study on erosion behavior of three types of superalloys through both experimental and numerical methods using multi-particle Finite Element Analysis (FEA) simulations. The investigated materials included GH4720Li, GH438, and GH4169, which were subjected to erosion by silica (SiO_2) particles. The study revealed that the particle impact angle significantly influenced the erosion outcomes for each material. Moreover, the simulation results closely matched those obtained from the experimental investigations [13].

Zhang et al. (2017) investigated several parameters that affect erosion wear such as angle of attack, velocity, particle size, and material properties using three-dimensional finite element method (FEA). The study utilized Q345 material as the target material. Their findings revealed a direct correlation between the velocity of particles and their size, whereby an increase in velocity leads to a corresponding increase in the rate of erosion. Additionally, the study revealed a significant incease in the erosion rate at intermediate angles of attack, ranging from 20 to 50 degrees. The study by Xiao, et al. (2017) also showed that brittle materials tend to be more resistant to erosion at low impact speeds and angles of attack [14], [15].

Based on previous studies, extensive research has been conducted on the wear behavior of SKD11 tool steel, with primary emphasis on abrasive wear associated with its applications as cutting tools and die materials. However, the erosion behavior of SKD11, particularly under varying particle impact angles and velocities, has received comparatively limited attention. This study addresses this gap by numerically investigating the erosion response of SKD11 tool steel using a three-dimensional Finite Element Method, providing mechanistic insight into erosion damage that has not been adequately explored in prior abrasion-focused studies. By varying the angle of attack and particle impact velocity, this work aims to improve the understanding of the erosion resistance of SKD11 tool steel. Moreover, SKD11 has strong potential as an erosion-resistant material due to its high chromium content, which promotes the formation of chromium carbides known to enhance resistance against erosion [4].

2. Methods

2.1 Material Model

In this study, SKD 11 steel was selected as the target material subjected to erosion using the Cowper-Symonds Strain Rate Material Model. SKD 11 Alloy Steel (JIS-G4404 according to Japanese standards) is a steel that is commonly used as a mold material in metal forming processes. This Alloy Steel was chosen because it has good compressive strength and resistance to deformation [16], [17], [18]. A sand particle (SiO_2) with was chosen as the erodent particle in the simulation. Table 1 shows the material parameters used in the simulation. In order to reduce the simulation time, the erodent particle can be considered nondeformable.

To eliminate the influence of strain rate dependence in the material model, the Cowper-Symonds Strain Rate Material Model is used for modelling the material in the simulation. The model scales the initial yield stress (σy) by two factors. A strain factor and strain rate factor as shown in equation (1). Where the σ0 is the Initial yield stress, $\dot{\varepsilon}$ is the strain rate, C and P are the Cowper-Symonds strain rate parameters. β is the strain hardening parameter, ε_P^{eff} is the effective plastic strain, and EP is the plastic hardening modulus which are obtained by equation (2) [19].

Table 1. Material Parameters

Materials	Yield stress (GPa)	Tensile Strength (GPa)	Density (kg/mm3)	Young's modulus (GPa)	Poisson ratio
SKD11	0.688	0.786	8.4e-6	210	0.3
SiO2			2.2e-6	0.0731	0.15

$$\sigma_y=[1+(\dot{\varepsilon}/C)^{\frac{1}{P}}](\sigma_0+\beta E_P \varepsilon_P^{eff}) \quad \text{.....1}$$

$$E_P=\frac{E_{tan}E}{E-E_{tan}} \quad \text{.....2}$$

2.2 Geometry and Mesh

In this study, a three-dimensional FEA model was prepared to further understand the erosion behaviour of SKD 11 steel material at three different angles of attack and two different impact velocities. In the simulation. a 0.7 mm erodent particle was used and the eroded target material had dimensions of 1x1x0.5 mm to speed up the simulation time. The erodent particle velocity was varied to 25 m/s and 50 m/s. Three variations of particle attack angles were also used including 30, 60, and 90 degrees.

In a Finite Element Analysis method, the mesh works by dividing the model into smaller elements that are important for the mathematical model to solve the equations correctly so that the data obtained is accurate [12]. To obtain accurate and reliable results, five variations of mesh element density namely 62,500, 256,000, 500,000, 106 and 1.5x106 elements were analyzed in the Mesh Independence Study. The illustration and mesh details of the model used are shown in Figure 1.

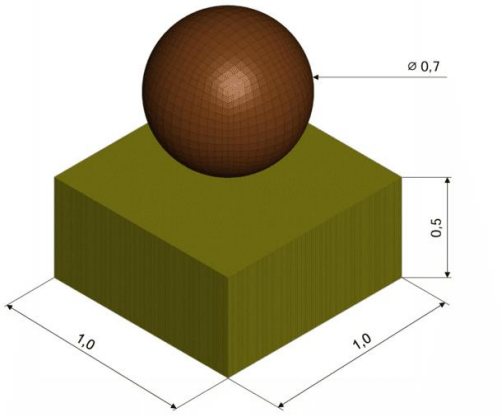

Figure 1. Geometry and Mesh of the Model

2.3 Mesh Convergence Study

A mesh convergence study is essential in numerical simulations to ensure that the results obtained are not significantly influenced by the mesh density used in the model [12], [20]. In this study, five different mesh densities were tested: 62,500; 256,000; 500,000; 1,000,000; and 1.5×10^6 elements. The mesh convergence analysis was performed by comparing the maximum effective stress (von Mises stress) values across these mesh variations. Based on the results, the model with 1 million elements was selected for subsequent simulations, as it exhibited a small error margin of 0.73% compared to the 1.5 million-element mesh, while offering significantly faster computation time. Figure 2 provides a more detailed illustration of the mesh independence study results.

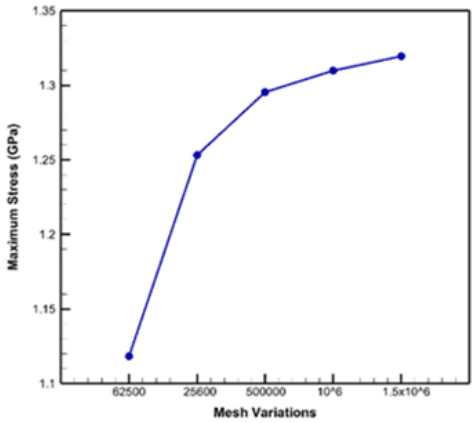

Figure 2. Mesh Convergence Study Results

3. Results and Discussion

3.1 Effective-stress (Von-Misses)

Figure 3(a) illustrates the maximum von Mises stress values of each material over time under three different impact angles, with a constant particle velocity of 25 m/s. A consistent trend is observed across all materials, in which lower impact angles generate higher maximum stress values. This behavior is attributed to the longer contact duration between the impacting particles and the material surface at lower angles, which plays a significant role in governing the surface response during erosion. The particle–surface contact duration can also be inferred from the stress-time curves, where a sharp drop in the maximum von Mises stress indicates the termination of contact [22]. Based on these results, the longest contact time occurs at an impact angle of 30°, followed by 60°, while the shortest contact time is observed at 90°.

Figure 3(b) shows the stress contour at an impact angle of 30°, where stress concentration is observed to align with the direction of particle motion. At an impact angle of 60°, as shown in Figure 3(c), the stress remains oriented along the particle trajectory but is distributed over a broader area. In contrast, Figure 3(d) presents the stress distribution at a 90° impact angle, where the stress is concentrated perpendicular to the surface and localized at the center of the impact zone. These results indicate that increasing the impact angle leads to a wider and more symmetric distribution of stress across the material surface. Such variations in stress distribution directly influence the dominant erosion mechanisms at different impact angles. At shallow impact angles, erosion is primarily governed by micro-cutting mechanisms, whereas at higher impact angles, the erosion process is dominated by crater formation and localized plastic deformation [23], [24].

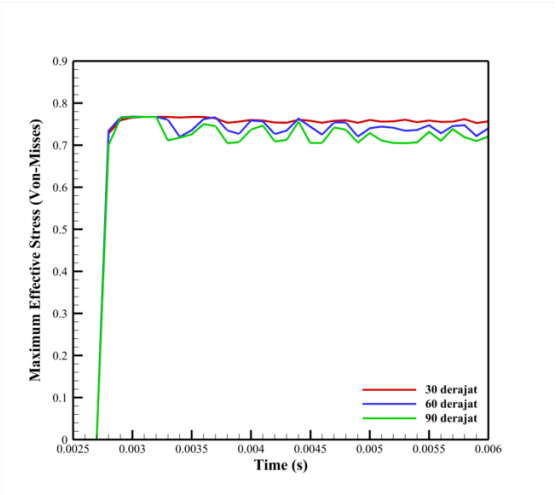

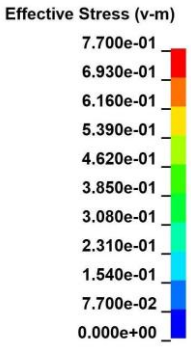

(a) Graph of Maximum Von Mises Stress

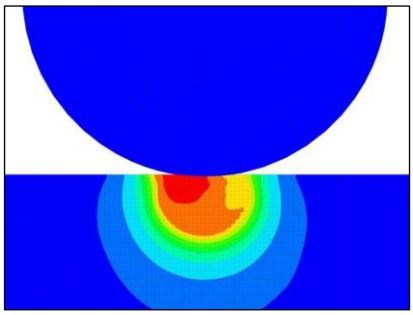

(b) Stress Contour at 30-Degree Impact Angle

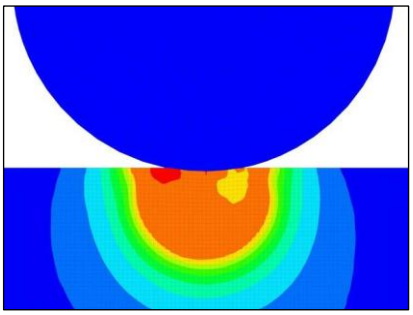

(c) Stress Contour at 60-Degree Impact Angle

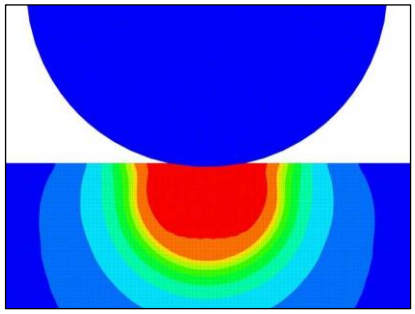

(d) Stress Contour at 90-Degree Impact Angle

Figure 3. Maximum Effective Stress

3.2 Maximum Effective Plastic Strain

Figure 4 presents the maximum plastic strain for various combinations of particle velocity and impact angle. At a particle velocity of 25 m/s, the material primarily undergoes plastic deformation without noticeable material loss. Under this condition, the plastic strain increases significantly as the impact angle rises from 30° to 60°, reaching a maximum at 60°, and then decreases at 90°. In contrast, at a higher particle velocity of 50 m/s, surface failure and material removal dominate the response of the material. Consequently, the differences in plastic strain across the impact angles become relatively small, with only a slight increase observed as the impact angle increases. This behavior indicates that, at higher velocities, the influence of impact angle on plastic strain is diminished. These findings are consistent with the work of Okonkwo et al. [25], who reported that increasing particle velocity significantly enhances the erosion rate of materials, particularly at shallow impact angles.

3.3 Eroded Volume

When abrasive particles (SiO_2) impact the target material (SKD11) at a velocity of 50 m/s, the surface of the target undergoes material failure, resulting in erosion and material detachment. Figure 5 illustrates the eroded volume at various particle impact angles. A substantial increase in eroded volume is observed as the impact angle increases from 30° to 60°. With a further increase to 90°, the eroded volume continues to rise; however, the rate of increase becomes less pronounced. This trend is consistent with the variation in maximum effective plastic strain at a particle velocity of 25 m/s, as shown in Figure 4. Previous studies have reported that the maximum effective plastic strain is directly correlated with the erosion behavior of materials, supporting the observed relationship between plastic deformation and erosion severity in this study [1], [3], [15].

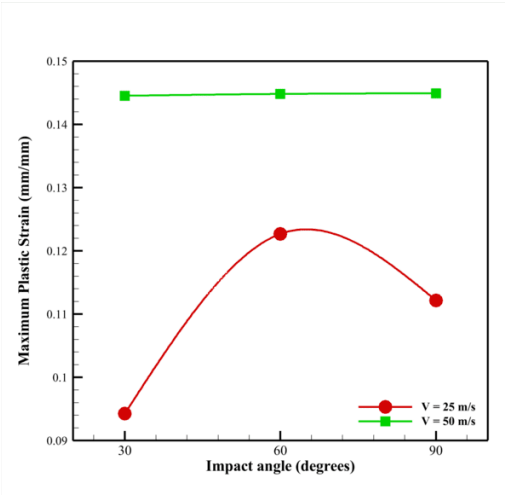

Figure 4. Maximum plastic strain

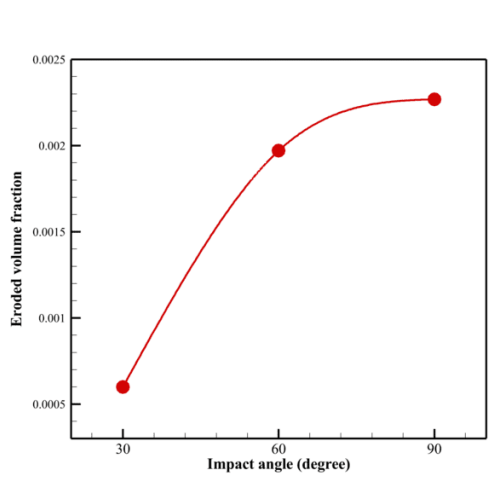

Figure 5. Eroded volume fraction

3.4 Surface Deformation of the Model

Figure 6 illustrates the surface deformation of the material induced by particle impact. Figures 6(a), 6(b), and 6(c) show the deformation profiles at impact angles of 30°, 60°, and 90°, respectively, for particles traveling at a velocity of 25 m/s. The results indicate that the magnitude of surface deformation increases with increasing impact angle, reaching a maximum at 90°. At impact angles of 30° and 60°, the deformation is not oriented perpendicular to the material surface but instead follows the particle trajectory, which is consistent with the stress distribution patterns previously shown in Figure 3.

Figures 6(d), 6(e), and 6(f) illustrate the material deformation at impact angles of 30°, 60°, and 90°, respectively, for particles impacting at a velocity of 50 m/s. At this higher velocity, surface failure accompanied by material erosion is clearly observed. At an impact angle of 30°, as shown in Figure 6(d), erosion remains relatively shallow; however, the oblique impact causes particle trajectory deflection, which pushes material along the direction of particle motion. This process promotes the formation of cutting lips on the material surface, as highlighted in Figure 6(g) [26].

At an impact angle of 60°, particles penetrate more deeply into the target surface, resulting in the displacement of a larger material volume along the particle trajectory (Figure 6(e)). This intermediate angle leads to the simultaneous formation of craters and cutting lips, as illustrated in Figure 6(h) [27].

In contrast, at a normal impact angle of 90°, the particles strike the surface perpendicularly without trajectory deflection, producing the deepest crater among all tested angles, as shown in Figure 6(f). Under this condition, crater formation dominates and cutting lips are absent, which is a behavior distinct from that observed at lower impact angles. The detailed crater morphology is presented in Figure 6(i) [28].

4. Conclusion

This study investigated the erosion response and damage mechanisms of SKD11 tool steel under varying particle impact angles and velocities using the Finite Element Method. The results demonstrate that impact angle plays a critical role in governing plastic deformation and erosion severity, with the lowest damage observed at a shallow impact angle of 30°. As the impact angle increases to 60°, plastic deformation and erosion intensify due to enhanced material displacement, while further increasing the angle to 90° shifts the dominant response toward localized crater formation. In addition, higher particle velocity significantly accelerates surface damage, promoting the transition from plastic deformation to material removal.

The study identifies distinct erosion mechanisms of *cutting lip* formation at shallow angles, a crater dominated erosion at normal impact, and a mixed mechanism at intermediate angles highlighting the strong coupling between impact kinematics and material response. This model provides a foundation for future development toward multi-particle erosion simulations and experimental validation, enabling more realistic prediction of erosion behavior in practical engineering applications.

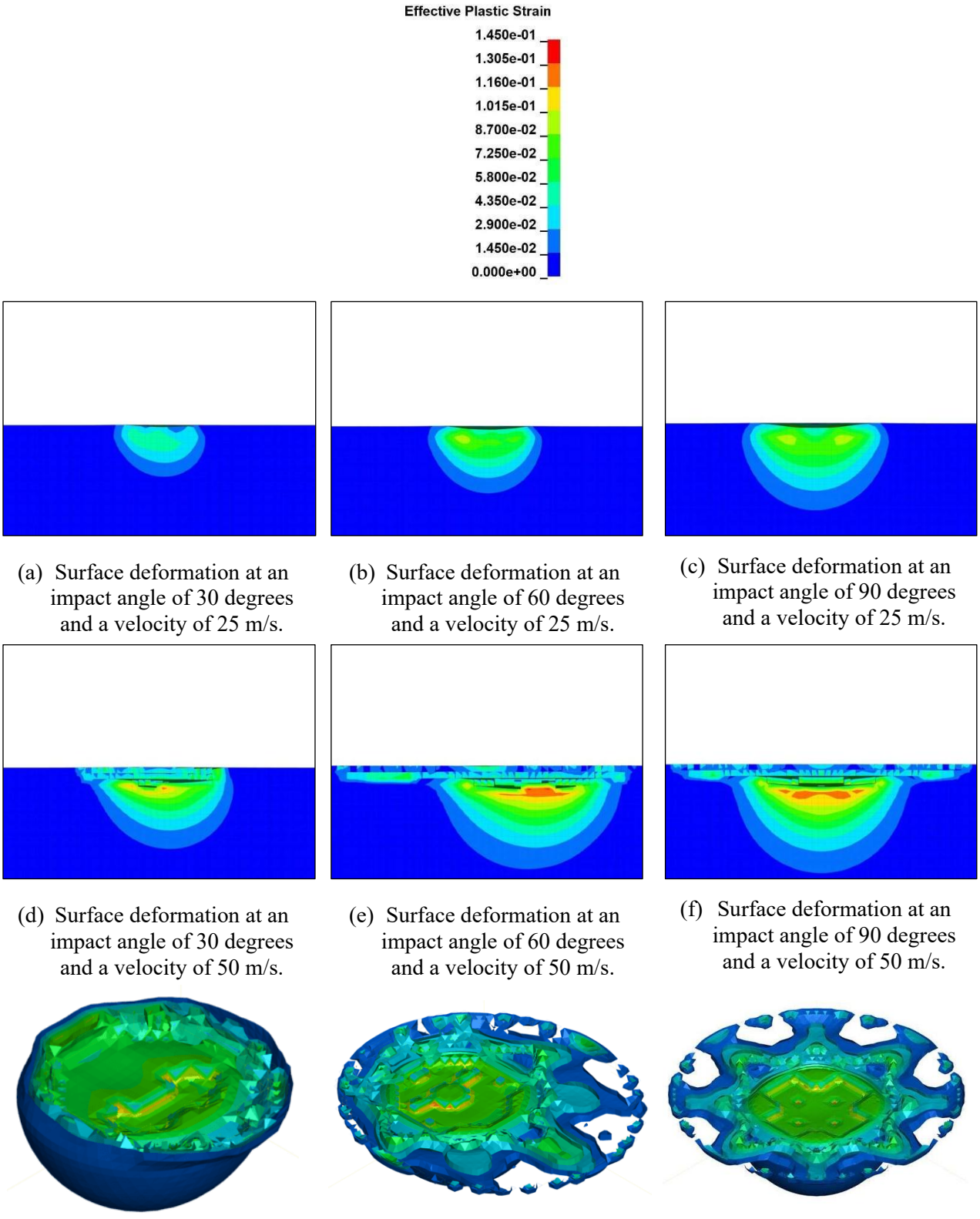

(a) Surface deformation at an impact angle of 30 degrees and a velocity of 25 m/s.

(b) Surface deformation at an impact angle of 60 degrees and a velocity of 25 m/s.

(c) Surface deformation at an impact angle of 90 degrees and a velocity of 25 m/s.

(d) Surface deformation at an impact angle of 30 degrees and a velocity of 50 m/s.

(e) Surface deformation at an impact angle of 60 degrees and a velocity of 50 m/s.

(f) Surface deformation at an impact angle of 90 degrees and a velocity of 50 m/s.

(g) Eroded surface at an impact angle of 30 degrees.

(h) Eroded surface at an impact angle of 60 degrees.

(i) Eroded surface at an impact angle of 90 degrees.

Figure 6. Plastic Deformation at the Surface of the Material

References

[1] K. Shimizu *et al.*, "Microstructural evaluation and high-temperature erosion characteristics of high chromium cast irons," *Wear*, vol. 426, pp. 420–427, 2019.

[2] I. Finnie, "Erosion of surfaces by solid particles," *wear*, vol. 3, no. 2, pp. 87–103, 1960.

[3] K. Kusumoto, K. Shimizu, R. H. Purba, and Y. Momma, "Effect of carbide refinement on high temperature erosive wear behavior of high chromium white cast iron with different titanium and carbon additions," *Mater Today Commun*, vol. 39, p. 109276, 2024.

[4] M. A. S. bin Abdul Rahim, M. bin Minhat, N. I. S. B. Hussein, and M. S. bin Salleh, "A comprehensive review on cold work of AISI D2 tool steel," *Metallurgical Research & Technology*, vol. 115, no. 1, p. 104, 2018.

[5] D.-C. Wen, "Erosion and wear behavior of nitrocarburized DC53 tool steel," *Wear*, vol. 268, no. 3–4, pp. 629–636, 2010.

[6] D. C. Wen, "Effect of nitrocarburizing time on the microstructures and erosion behavior of cold-work tool steel," *ISIJ international*, vol. 49, no. 11, pp. 1762–1768, 2009.

[7] S.-H. Chang, C.-C. Yu, K.-T. Huang, and C.-M. Liu, "Deposition of DLC/oxynitriding Films onto JIS SKD11 Steel by Bipolar-pulsed PECVD," *ISIJ International*, vol. 55, no. 12, pp. 2631–2638, 2015.

[8] S. Cho, I. Jo, H. Kim, H.-T. Kwon, S.-K. Lee, and S.-B. Lee, "Effect of TiC addition on surface oxidation behavior of SKD11 tool steel composites," *Appl Surf Sci*, vol. 415, pp. 155–160, 2017.

[9] J. L. Li, L. L. Jing, and M. Chen, "An FEM study on residual stresses induced by high-speed end-milling of hardened steel SKD11," *J Mater Process Technol*, vol. 209, no. 9, pp. 4515–4520, 2009.

[10] M. Du, Z. Li, L. Feng, X. Dong, J. Che, and Y. Zhang, "Numerical simulation of particle fracture and surface erosion due to single particle impact," *AIP Adv*, vol. 11, no. 3, 2021.

[11] M. Ngqase and X. Pan, "An overview on types of white cast irons and high chromium white cast irons," in *Journal of Physics: Conference Series*, IOP Publishing, 2020, p. 012023.

[12] H. Patil and P. V Jeyakarthikeyan, "Mesh convergence study and estimation of discretization error of hub in clutch disc with integration of ANSYS," in *IOP conference series: materials science and engineering*, IOP Publishing, 2018, p. 012065.

[13] X. Yaer, K. Shimizu, J. Qu, B. Wen, X. Cao, and K. Kusumoto, "Surface deformation micromechanics of erosion damage at different angles and velocities for aero-engine hot-end components," *Wear*, vol. 426, pp. 527–538, 2019.

[14] C. Zheng, Y. Liu, C. Chen, J. Qin, and S. Zhang, "Finite element analysis on the dynamic erosion process using multiple-particle impact model," *Powder Technol*, vol. 315, pp. 163–170, 2017.

[15] L. Xiao, K. Shimizu, and K. Kusumoto, "Impact angle dependence of erosive wear for spheroidal carbide cast iron," *Mater Trans*, vol. 58, no. 7, pp. 1032–1037, 2017.

[16] C. Wang, Y. Xie, L. Zheng, Z. Qin, D. Tang, and Y. Song, "Research on the chip formation mechanism during the high-speed milling of hardened steel," *Int J Mach Tools Manuf*, vol. 79, pp. 31–48, 2014.

[17] C. Wang, F. Ding, D. Tang, L. Zheng, S. Li, and Y. Xie, "Modeling and simulation of the high-speed milling of hardened steel SKD11 (62 HRC) based on SHPB technology," *Int J Mach Tools Manuf*, vol. 108, pp. 13–26, 2016.

[18] T.-B. Mac, T.-T. Luyen, and D.-T. Nguyen, "A Study for improved prediction of the cutting force and chip shrinkage coefficient during the SKD11 alloy steel milling," *Machines*, vol. 10, no. 4, p. 229, 2022.

[19] C. Hernandez, A. Maranon, I. A. Ashcroft, and J. P. Casas-Rodriguez, "A computational determination of the Cowper–Symonds parameters from a single Taylor test," *Appl Math Model*, vol. 37, no. 7, pp. 4698–4708, 2013.

[20] J. Julian, W. Iskandar, F. Wahyuni, and F. Ferdyanto, "Computational fluid dynamics analysis based on the fluid flow separation point on the upper side of the naca 0015 airfoil with the coefficient of friction," *Media Mesin: Majalah Teknik Mesin*, vol. 23, no. 2, pp. 70–82, 2022.